Devil's staircase between antiferroelectric SC_A^* and ferroelectric SC* phases in liquid crystals observed in free-standing films under temperature gradients

Keizo Itoh,[a] Masaaki Kabe,[b] Kouichi Miyachi,[b] Yoichi Takanishi,[b] Ken Ishikawa,[b] Hideo Takezoe[b] and Atsuo Fukuda*[b]

[a]*Kashima Oil Co. Ltd., R & D Department, Towada, Kamisu-machi, Kashima-gun, Ibaraki 314-02, Japan*

[b]*Tokyo Institute of Technology, Department of Organic and Polymeric Materials, O-okayama, Meguro-ku, Tokyo 152, Japan*

By studying the electro-optical properties and the textures of the subphases successively emerging between antiferroelectric SC_A^* and ferroelectric SC* (the Devil's staircase), we have revealed several interface effects in both homogeneous and homeotropic cells; free-standing films are most suitable for making observations almost free from the effects. By applying appropriate temperature gradients to the free-standing films, we can directly see any part of the subphase sequence in the visual field of an optical microscope. The two ferrielectric subphases on the low- and high-temperature sides of ferrielectric SC_γ^* together with another ferrielectric subphase between the antiferroelectric subphase (designated as AF in ref. 9) and SC* were thus confirmed to exist definitely. We have discussed the origin of these successive subphases in terms of the several theoretical models reported so far, concluding that the ANNNI model with the third-nearest-neighbour interaction well describes their Devil's staircase character.

Various tilted, chiral, fluid smectic (SC*-like) phases have been found in antiferroelectric liquid crystals,[1,2] which are shown in Scheme 1 in increasing order of temperature; some of the phases may not actually occur but, when they do exist, they follow this order in almost all the compounds and mixtures investigated so far.[1–25] The SC_A^* and SC* phases are the fundamental ones and the others between them, together with SC_α^*, are the subphases. Ferrielectric SC_γ^* and antiferroelectric AF phases seem to be secondarily fundamental.[8–11] On the high- and low-temperature sides of SC_γ^*, there may emerge ferrielectric FI_H and FI_L phases, respectively.[8–11] The existence of FI, another ferrielectric subphase between AF and SC*, was reported recently by Hatano *et al.*[13] and O'Sullivan *et al.*[21] Isozaki *et al.*[9] insisted that a few additional subphases seem to emerge in the vicinity of FI_H and FI_L. Likewise, some subphases other than FI are expected in the temperature region between AF and SC*. Consequently, we designated these regions as spr1, spr2 and spr3, respectively, where spr refers to subphase region.

There are three factors that may apparently confuse the above sequence. First, the rather stable antiferroelectric AF phase appearing in addition to SC_A^* may cause inappropriate identification of AF to SC_A^*. Secondly, ferroelectric tilted hexatic SI* below SC_A^* may cause inappropriate identification of SI* to SC*.[25] Thirdly, the staircase character of SC_α^* described in the following may complicate the situation, particularly when SC* does not emerge. The fourth complexity is rather essential and is due to substrate interfaces which sometimes influence the subphase appearances considerably.

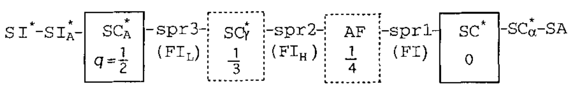

Scheme 1 A possible, most general subphase sequence in antiferroelectric liquid crystals

Among these subphases, SC_α^* is quite different from the other ones between SC_A^* and SC* in the sense that it is located above SC*. In previous papers,[2,22–24] we reported that SC_α^* forms not only the electric-field-induced staircase, SC_α^* (q_E), but also the temperature-induced one, SC_α^* (q_T). However, the staircase characters are not so typical to allow us meaningful comparison between theory and experiment. We have also conjectured that the subphases emerging between SC_A^* and SC* form another temperature-induced staircase describable by the one-dimensional Ising model with long-range repulsive interactions.[2,8–11,26–28] Since some other theoretical explanations have also been published,[29–53] it is appropriate to investigate the subphases experimentally in more detail and to examine the applicability of the proposed theoretical models. We expect that this staircase will appear much more typical so that the investigation and the examination will be performed practically, if thick free-standing films[54–56] of suitable materials are prepared carefully. The purposes of this paper are: (1) to establish a convenient method of studying the staircase between SC_A^* and SC*; (2) to introduce some suitable materials which allow us to characterize unambiguously the subphases in the regions spr3, spr2 and spr1; (3) to discuss the origin of the staircase in terms of the several theoretical models so far proposed; and (4) to conclude that the ANNNI model with the third-nearest-neighbour interaction (ANNNI + J_3 model)[29–34,36] describes well the Devil's staircase character of the subphases between SC_A^* and SC*.†

Experiment

Three antiferroelectric liquid crystal compounds were used in this experiment, the structural formulae of which are summar-

† The molecular orientational structures are specified by q_T in the one-dimensional Ising model with long-range repulsive interactions[2] and by q in the ANNNI + J_3 model.[29–34] Both of the models assign essentially the same structures to SC_A^* ($q=1/2$, $q_T=0$), SC_γ^* ($q=1/3$, $q_T=1/3$), AF ($q=1/4$, $q_T=1/2$) and SC* ($q=0$, $q_T=1$) but may predict different ones for subphases in spr3, spr2 and spr1.

ized in Scheme 2. Homogeneously aligned samples were prepared by rubbing polyimide (Toray, SP510) spin-coated on glass substrate plates with indium tin oxide (ITO) electrodes. Homeotropically aligned samples were also prepared between glass substrate plates coated with silane coupling agents (Toray Dow Corning Silicone, AY 43-021). Polyester (PET) films were used as spacers in both homogeneous and homeotropic cells. Free-standing film samples were formed in a 1.5×8 mm^2 rectangular hole of a glass frame depicted in Fig. 1. The film thickness was estimated at *ca.* 100 μm from the upper and lower film surfaces pinpointed with an optical microscope. An electric field can be applied parallel to the 1.5 mm edges using two ITO electrodes prepared along the 8 mm edges. The frame has another ITO heater electrode on the right side, which can produce a temperature gradient in the free-standing film sample. Samples aligned in a homogeneous/homeotropic cell or prepared as a free-standing film were mounted in an oven and the temperature was controlled with an accuracy of ±10 mK.

Texture observation and electro-optical switching investigation were performed using the same system as described in previous papers.[1,2,22–24] The helicoidal pitch multiplied by the average refractive index was determined by observing the transmittance loss due to selective reflection using a spectrophotometer (Hitachi, U-3410). Laser light diffraction patterns were obtained by the same system as used in photon correlation spectroscopy with a He–Ne laser and a goniometer.[57] Fig. 2 illustrates a system for obtaining conoscopic figures by applying an electric field to unwind the helicoidal structure. Its details have already been reported in ref. 58, apart from one improvement which is essential in the present investigation using free-standing films under temperature gradients; an eyepiece together with a beam splitter was added, so that by the use of backward illumination, we can pin-point the sample area where the conoscopic observation occurs.

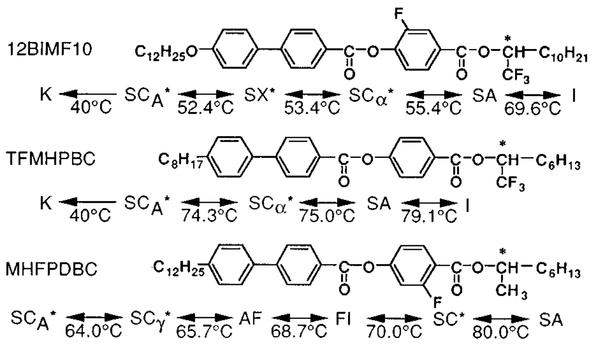

Scheme 2 Compounds used and their phase sequences outlined roughly. Note that substrate interfaces sometimes influence not only the transition temperatures but also the phase appearances themselves

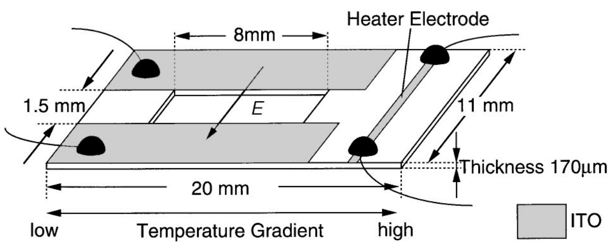

Fig. 1 Frame for a free-standing film and holder for producing temperature gradients

Results

12BIMF10 homogeneous cells

Plate 1 shows micrographs of a 6 μm thick 12BIMF10 cell aligned homogeneously by polyimide (Toray, SP510) rubbing. When the phase transition from SA to the unidentified SX_1* phase occurs, needle-like defects emerge perpendicular to the smectic layer, but fringe lines parallel to the smectic layer, indicating a helicoidal structure, do not appear; the extinction directions are parallel and perpendicular to the smectic layer. These are the characteristic features of SC_α* and hence SX_1* must be SC_α*. On cooling to another unidentified phase SX_2*, both focal conics and fringe lines parallel to the smectic layer, indicating the helicoidal structure, appear and light transmission occurs slightly even when the crossed polarizers are set at extinction directions parallel and perpendicular to the smectic layer; this SX_2* texture looks like that of SC_γ*. As the temperature decreases further, SC_A* appears.

The switching currents observed in the same cell at various temperatures by applying a 0.5 Hz, ±6 V μm^{-1} triangular wave are shown in Fig. 3. In the high-temperature region of SX_1*, two current peaks were observed, suggesting the antiferroelectric character of SX_1*; the number of current peaks increases with the decrease of temperature in SX_1*. This switching behaviour, together with the texture illustrated in Plate 1, almost unambiguously identifies SX_1* as SC_α*. After the phase transition to SX_2*, five current peaks were observed; the number of current peaks remains five in SX_2*. Since three peaks are expected to appear in SC_γ*, it is not reasonable to simply identify SX_2* as SC_γ*.

Fig. 4 summarizes the laser light diffraction patterns obtained at various temperatures covering SA, SX_1*, SX_2* and SC_A* in a 350 μm thick 12BIMF10 cell aligned homogeneously using a 1 T magnetic field. The phase-transition temperatures are different from those in Fig. 3, because they depend on the cell thickness and surface treatment. In both SA and SX_1*, no diffraction peaks emerge and the background lines are sufficiently low and almost noiseless; this was particularly true after all our effort to detect the diffraction peaks in SX_1* by changing the temperature at 0.1 °C intervals. When the phase transition to SX_2* occurs at 54.9 °C, the background lines become very high and noisy and two broad diffraction peaks emerge. The dashed line in Fig. 4 shows the zero level line of the diffraction observed at 54.9 °C. The large-angle diffraction peak moves toward the small-angle side with decreasing temperature, while the small-angle diffraction peak scarcely shows any temperature variation. The two diffraction peaks at the highest temperature in SX_2* correspond to periodicities 2.1 and 0.8 μm, which are not in the relation of the first- and second-order diffraction peaks.

12BIMF10 homeotropic cells

As described above, at least SX_2* appears to be affected considerably by substrate interfaces in homogeneous cells. Hence we tried to observe the Bragg reflection due to the

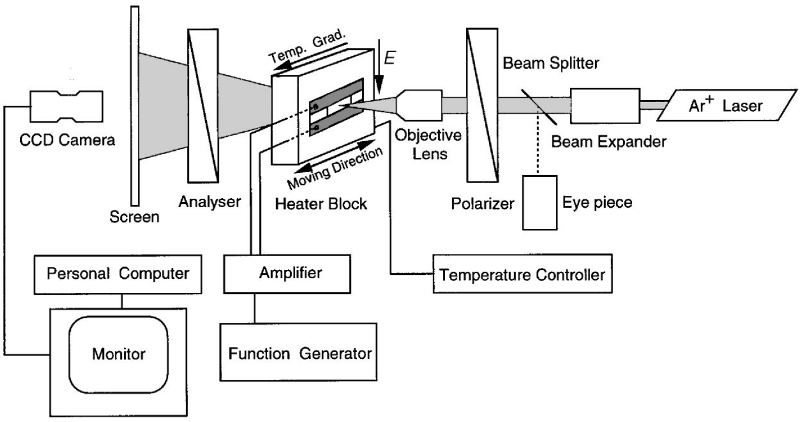

Fig. 2 Schematic illustration of the optical system for observing conoscopic figures

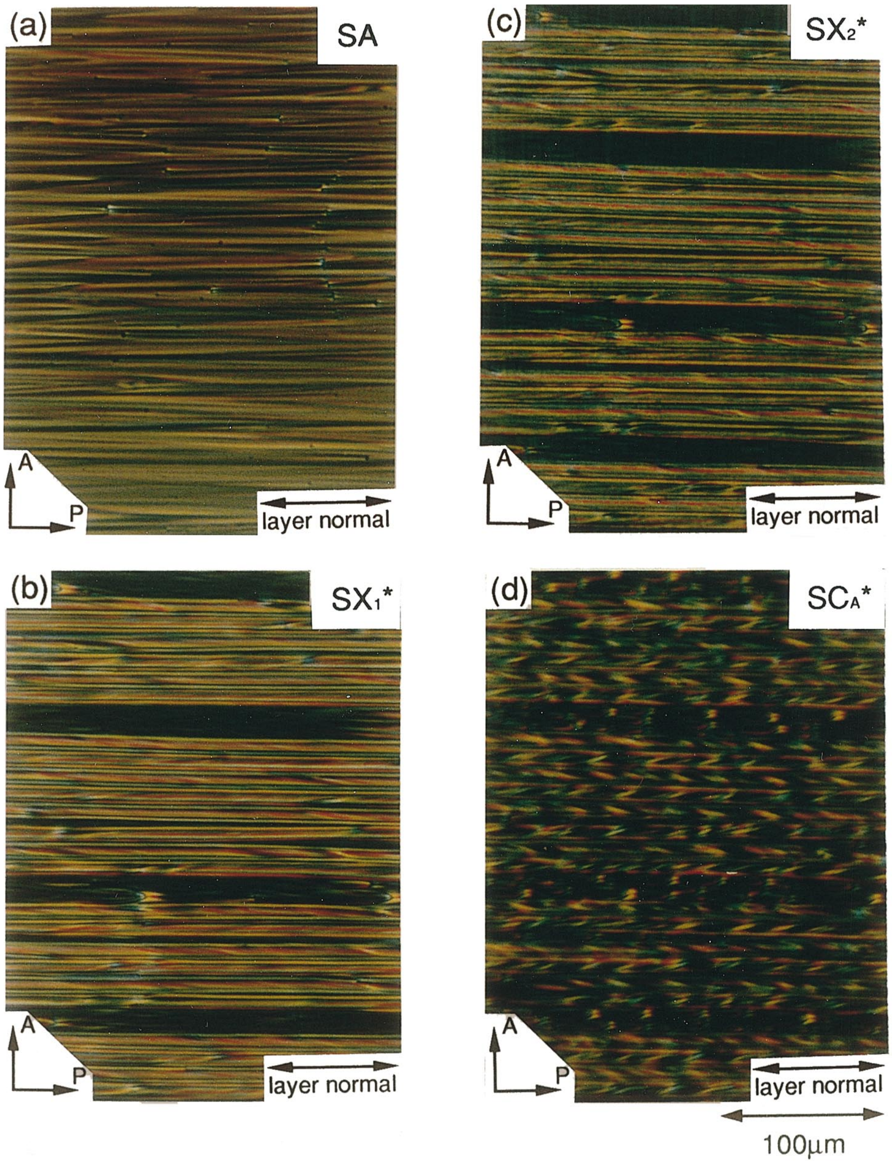

Plate 1 Micrographs of a 6 μm thick, 12BIMF10 cell homogeneously aligned by polyimide (Toray, SP510) rubbing

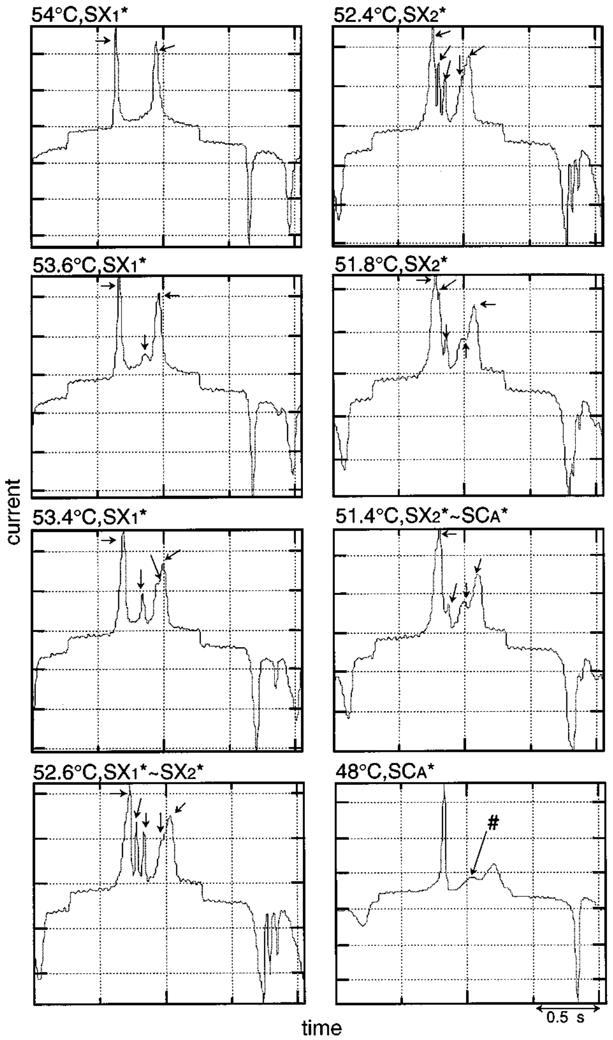

Fig. 3 Switching current observed in the same cell as used in Plate 1 at various temperatures by applying a 0.5 Hz, ± 6 V μm^{-1} triangular wave electric field. The peak indicated by # is due to flow of accidentally contained ions

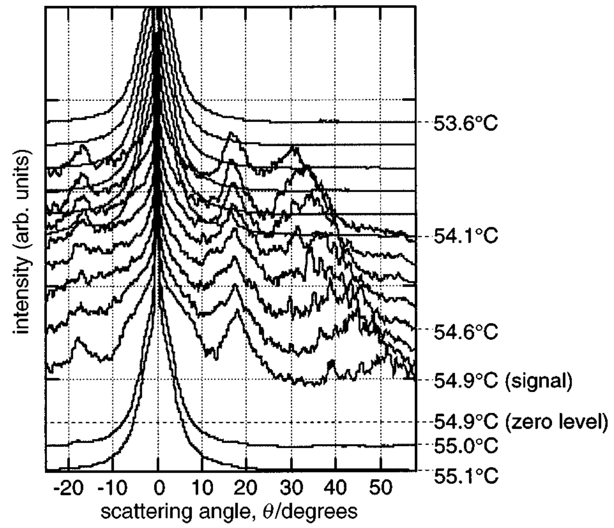

Fig. 4 Laser light diffraction patterns obtained at various temperatures in a 350 µm thick, 12BIMF10 cell aligned homogeneously using a magnetic field. The patterns are shown at 0.1 °C intervals and their ordinate zeros are shifted upwards constantly by one division

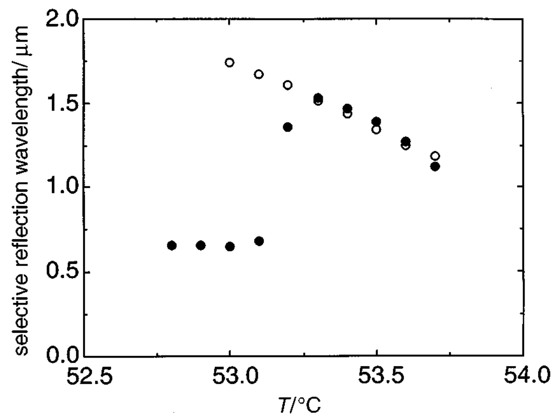

Fig. 5 Temperature variation (○, cooling; ●, heating) of Bragg-reflected peaks observed in a 100 µm thick, 12BIMF10 cell homeotropically aligned by surfactant (Toray Dow Corning Silicone, AY 43-021)

helicoidal structure in a 100 µm thick homeotropic cell. The results exceeded expectation and a beautiful Bragg reflection was observed; Fig. 5 shows the temperature variation of the reflected peak. The helicoidal pitch in SC_A* must be very short so that the corresponding Bragg reflection could not emerge in the transparent region of 12BIMF10. On heating to SX_2*, a red colouration was visible and a Bragg refection peaking at *ca.* 600 nm appeared. On further heating, the peak showed a steep increase to *ca.* 1.5 µm and then decreased slightly; SX_2* consists of at least two subphases. After the phase transition from SX_2* to SX_1*, no Bragg reflection was observed. In a cooling process, SX_2* behaved similarly in the high-temperature region, but hysteresis was observed and the 600 nm Bragg reflection did not appear in the low-temperature region. The 1.5 µm peak nearly corresponds to the periodicity producing the diffraction peak in Fig. 4 which shifts from 50° to 30° with decreasing temperature.

12BIMF10 free-standing films

In this way, homeotropic cells are much more ideal than homogeneous cells from the viewpoint that some subphase structures are realized easily. Still, the hysteresis and the disappearance of the red reflection in the low-temperature region suggest some influence exerted by substrate interfaces. To be as free from this influence as possible, we observed the subphases in a *ca.* 100 µm thick free-standing film under a temperature gradient and obtained their conoscopic figures by applying an electric field. Plate 2 shows a micrograph under crossed polarizers and two conoscopic figures. Between SC_A* and SC_α*, there exist two ferrielectric phases which must correspond to SX_2*. The red Bragg reflection is clearly seen and, within this red region, a conoscopic figure illustrated on

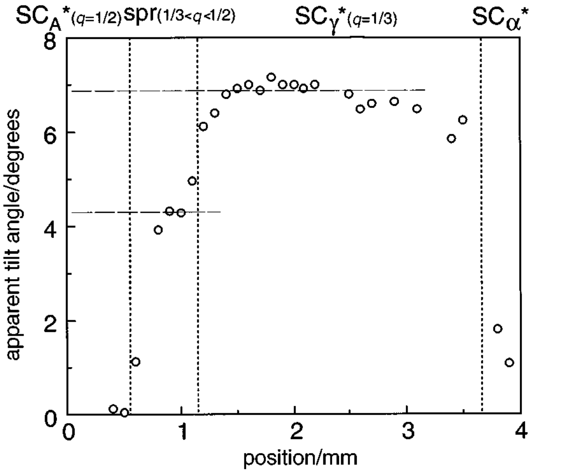

Fig. 6 Apparent tilt angle *vs.* temperature determined by measuring centre-shifts in the conoscopic figures under an applied electric field, 267 V mm^{-1}

the lower left is observed when an electric field high enough to unwind the helicoidal structure is applied. The region above (to the right of) the red one becomes dark because of the infrared Bragg reflection; a conoscopic figure illustrated on the right in the lower part is observed when unwinding the helicoidal structure. We saw the boundary between this dark region and SC_α*, although it is not clear in the plate.

We can determine the apparent tilt angle by measuring centre-shifts in the conoscopic figures as plotted in Fig. 6. The tilt angle is 21° in SC* produced from SC_A* by applying an electric field stronger than its threshold, and the two ferrielectric phases corresponding to the red and dark regions have apparent tilt angles of $4.2° \approx 21°/5$ and $6.9° \approx 21°/3$, respectively. Consequently, it is reasonable to assign the two ferrielectric subphases corresponding to SX_2*, which exhibit the red and infrared Bragg reflections, as subphases in spr3 and SC_γ*, respectively. Note that the Bragg reflection due to the helicoidal structure has not been observed in either of the subphases so far.

Free-standing films of TFMHPBC and MHFPDBC

To recognize properly the validity and limitation of the method using free-standing films under temperature gradients, we introduce two other materials, TFMHPBC and MHFPDBC, listed in Scheme 2, although the results obtained are rather preliminary. The TFMHPBC enantiomer has a simple phase sequence, where only SC_α* exists between SC_A* and SA, but its racemization complicates the phase sequence.[2,10] As far as the authors are aware, MHFPDBC is the only compound in which some subphase between AF and SC* has been reported to exist.[13] Quite recently, O'Sullivan *et al.* also reported a similar subphase in spr1 in another compound.[21]

Plate 3 shows a micrograph of a *ca.* 100 μm thick MHFPDBC free-standing film under a temperature gradient. We can see clearly the existence of at least one subphase in spr1. We were unable to observe its conoscope by applying an electric field, because some flow induced by the field occurred in SC* on the right side and disturbed the texture considerably. To avoid this flow, we stopped using the temperature gradient and tried to keep the film temperature uniform. On cooling, we first confirmed SC* by texture observation and then observed a conoscopic figure, which is clearly different from SC* and SC_A*; it looks like ferrielectric at 200 V mm^{-1} but antiferroelectric at 333 V mm^{-1} as shown in Plate 3. Consequently, we could not identify unequivocally the subphase in spr1 as ferrielectric.

Plate 4 shows micrographs and conoscopic figures of *ca.* 100 μm thick partially racemized TFMHPBC free-standing films. When the optical purity is $ee = (R-S)/(R+S) = 92\%$, both SC_γ* and another ferrielectric subphase in spr3, FI_L, were observed clearly between SC_A* and SC_α* as seen in Plate 4(*a*). The dark blue colour on the left side is caused by the Bragg reflection due to the SC_A* helicoidal structure; the SC_A* texture appears very uniform because the helicoidal pitch is short. The dark area on the right side represents SC_α*, the texture of which is always quite uniform in homogeneous cells as well as in free-standing films. The difference between the ferrielectric phases becomes much more clear if we observe conoscopic figures under an applied electric field of 17 V mm^{-1} as shown in Plate 4(*a*). When the optical purity was slightly reduced to $ee = (R-S)/(R+S) = 84\%$, three ferrielectric subphases, FI_L in spr3, SC_γ* and FI_H in spr2, and one antiferroelectric subphase, AF, were observed between SC_A* and SC_α* as seen in Plate 4(*b*).

As demonstrated in this and the preceding sections, free-standing films under temperature gradients are very effective for the direct observation of the subphases between SC_A* and SC*. When the helicoidal pitch is long, however, the film appearance may become disturbed and spurious phase boundaries may appear as illustrated in Plate 5. Even in such cases, conoscopic observation under an applied electric field can discriminate between the real and spurious phase boundaries. Among the several boundaries in the ferrielectric subphases, in fact, the lowest temperature boundary is the real one, because the conoscopic figures observed on both sides of this boundary are quite different, as shown in Plate 5.

Discussion

The successive phase transitions observed between ferroelectric SC* and antiferroelectric SC_A* can be regarded as the formation of large-scale structures in simple physical systems otherwise dominated by short-range forces. Some type of frustration must be present in those parts of the phase diagram where the structures are encountered. When the two dominant ordering forces of a system happen to compete with each other, a large number of alternative structures may have almost the same free energy. This degeneracy can be removed either by weak long-range forces or by thermal effects. The frustration at issue is the one between ferroelectricity and antiferroelectricity, *i.e.* the tilting correlation in adjacent layers, in the SC*-like phase; we would not expect to encounter such frustration, since it seems easy to lift any degeneracy by changing the molecular orientations in some way. In fact, the SC*-like phase has two degrees of freedom, the polar angle, θ, and the azimuthal angle, ϕ. Notwithstanding this, several theoretical treatments have been developed so far to understand the observed sequence of subphases based on the X–Y model.[41–53]

Possible antiferroelectric and ferrielectric structures induced by the multilayer tilt ordering from the parent SA have been constructed systematically on the basis of symmetry analysis.[51,52] To choose realistic structures for the most stable

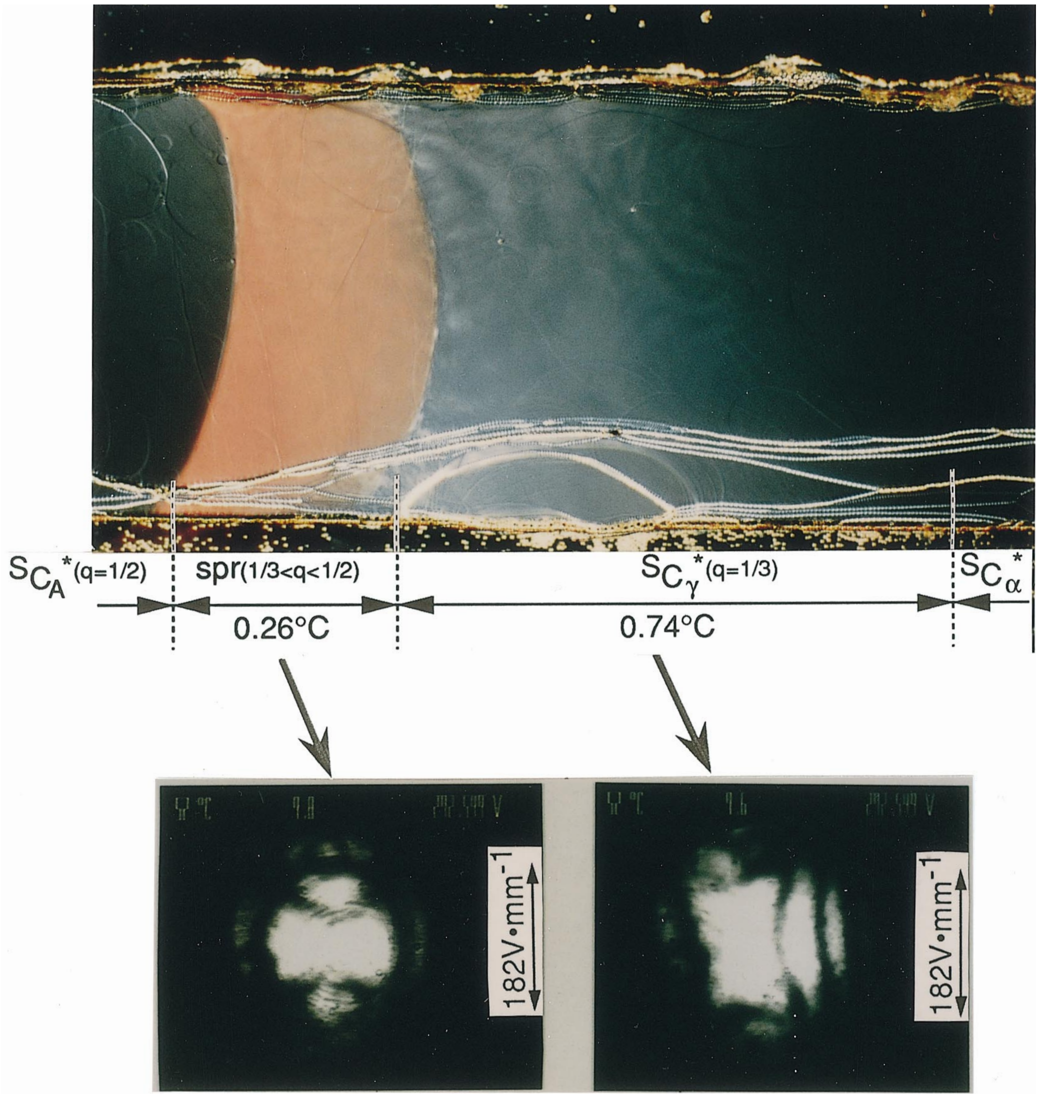

Plate 2 A micrograph of a *ca.* 100 μm thick, 12BIMF10 free-standing film under a temperature gradient and two conoscopic figures of a subphase in spr3 ($1/2>q>1/3$) and SC_γ* ($q=1/3$) under an applied electric field, 182 V mm^{-1}, sufficient to unwind the helicoidal structure. The q data presented in this and the following Plates have been determined by comparing the experimental observations with Yamashita's phase diagram reproduced in Fig. 7.

ferrielectric and antiferroelectric subphases, SC_γ* and AF, we naturally have to resort to several experimental facts. The first one is the temperature variation of the smectic layer spacing observed through the successive phase transitions; the spacing shows only a slight discontinuous change at the transitions, if any. Moreover, the diffraction peak does not show any change such as splitting. Consequently, the molecular tilt angles are practically constant, not only in a smectic layer but also from layer to layer; bilayer models with different tilt angles in adjacent layers[41,44,51] are impractical for SC_γ*. This fact is in accord with our intuition that smectics are one-dimensional crystal and the layer spacing change accompanies a large energy increase and hence seldom occurs. Empirically, once a tilt angle as large as 10° or more has been established, the electroclinic effect[59] is hardly observed.

The second experimental fact is that AF shows an LCICD (liquid-crystal-induced circular dichroism) due to the helicoidal structures.[60] Consequently, the n-layer ($n \geqslant 3$) spiral model[51,52] is not practical for AF, because the apparent n-fold symmetry diminishes biaxiality to such an extent that no optical rotatory power could be observed. The bilayer azimuthal mode model for SC_γ*[41,51] is not practical, either, because of the third and forth experimental facts that the biaxial optical plane orients parallel to the applied field[2,61] and that our recent X-ray experiment with synchrotron radiation revealed a Bragg reflection corresponding to three-layer spacing;[62] note that the bilayer azimuthal mode model needs to presuppose an azimuthal angle difference of *ca.* ±80° in adjacent layers and is unrealistic. Although the low-frequency dielectric properties have been reported to be well understood by the bilayer azimuthal mode model,[47] these characteristic properties can also be explained by the three-layer Ising model.[63]

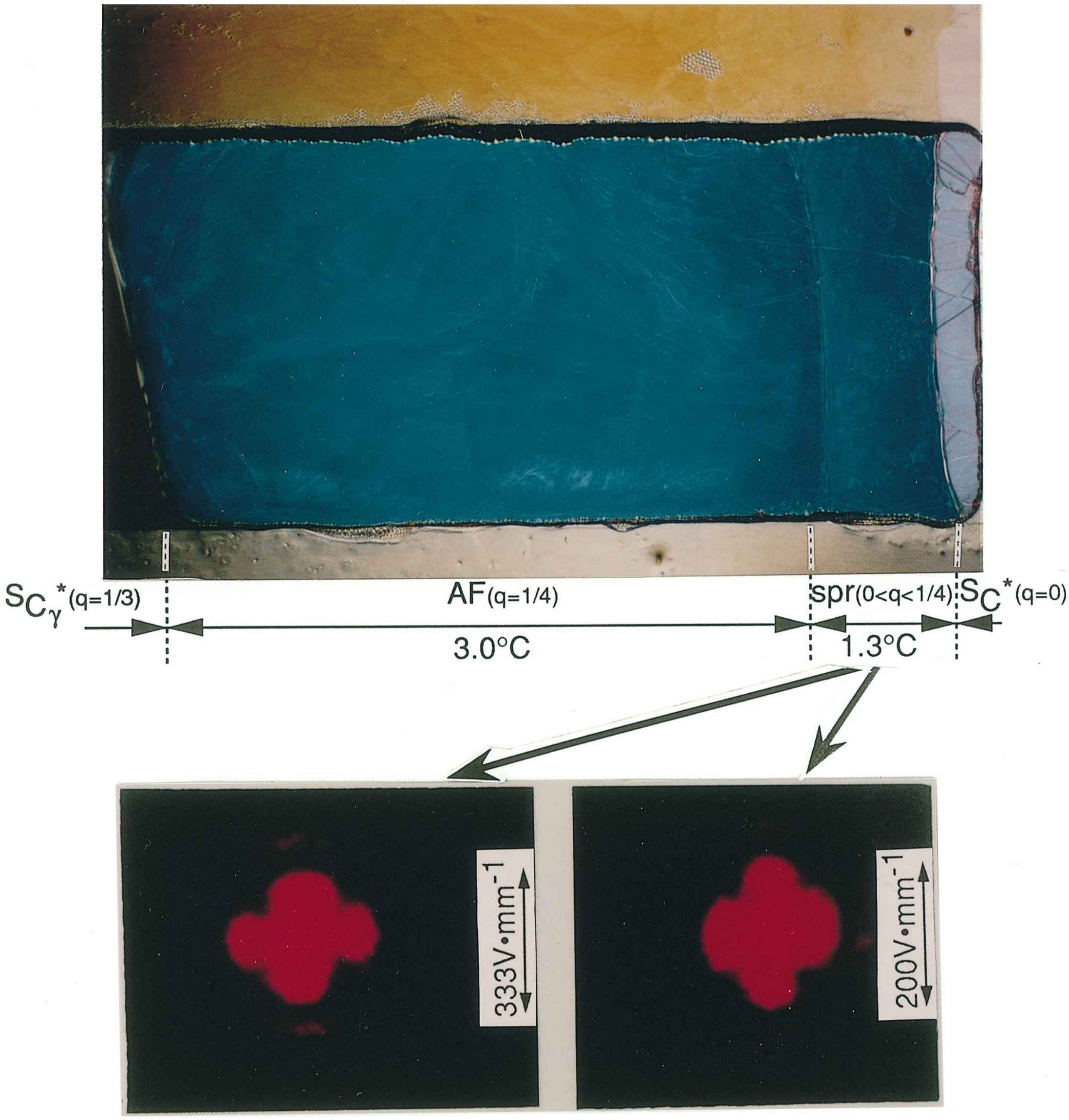

Plate 3 A micrograph of a *ca.* 100 μm thick, MHFPDBC free-standing film under a temperature gradient, and two conoscopic figures of a ferrielectric subphase in spr1 ($1/4>q>0$) under 200 and 333 V mm^{-1}; ferrielectric behaviour is shown at 200 V μm^{-1} and antiferroelectric behaviour is shown at 333 V μm^{-1}

The final experimental fact is well known but is very important. The helical pitch of antiferroelectric liquid crystals is fairly short compared with conventional ferroelectric liquid crystals. However, the chiral interaction is still so weak that the helicoidal pitch is very long as compared to the smectic layer spacing, *i.e.* the molecular length.[64] Consequently, the subphase sequence analysis based on the Landau-type phenomenological models should be performed carefully by taking account of the short-range interactions to produce large azimuthal angle changes between adjacent layers;[44,49,50] the existence of the short-range interaction has not been supported by any experimental evidence up until now. In this way, the Ising model appears to be most realistic. It should be noted that Phase II in Fig. 3 of the four-layer model and Phase III in Fig. 4 of the three-layer model in ref. 52 are effectively the same as the Ising model which we have already proposed;[2,9,65] note that the tilt (polar angle) is practically the same in the three layers (Phase III in Fig. 4) and Phase II in Fig. 3 exists practically even in the chiral case, because the helical structure is only a small perturbation caused by a weak interlayer chiral interaction.

What we would like to emphasize is the mechanism by which the tilting direction is restricted parallel to a plane both in ferroelectric SC* ($\phi=0$) and antiferroelectric SC_A* ($\phi=0$ or π). As mentioned above, we neglect the slight precession of at most a few degrees per layer caused by chirality. The excluded volume effect (the packing entropy effect) in a smectic layer structure preserving the density wave character must be the main factor that causes the molecules to tilt in the same direction and sense in SC*. Either of the two models based on

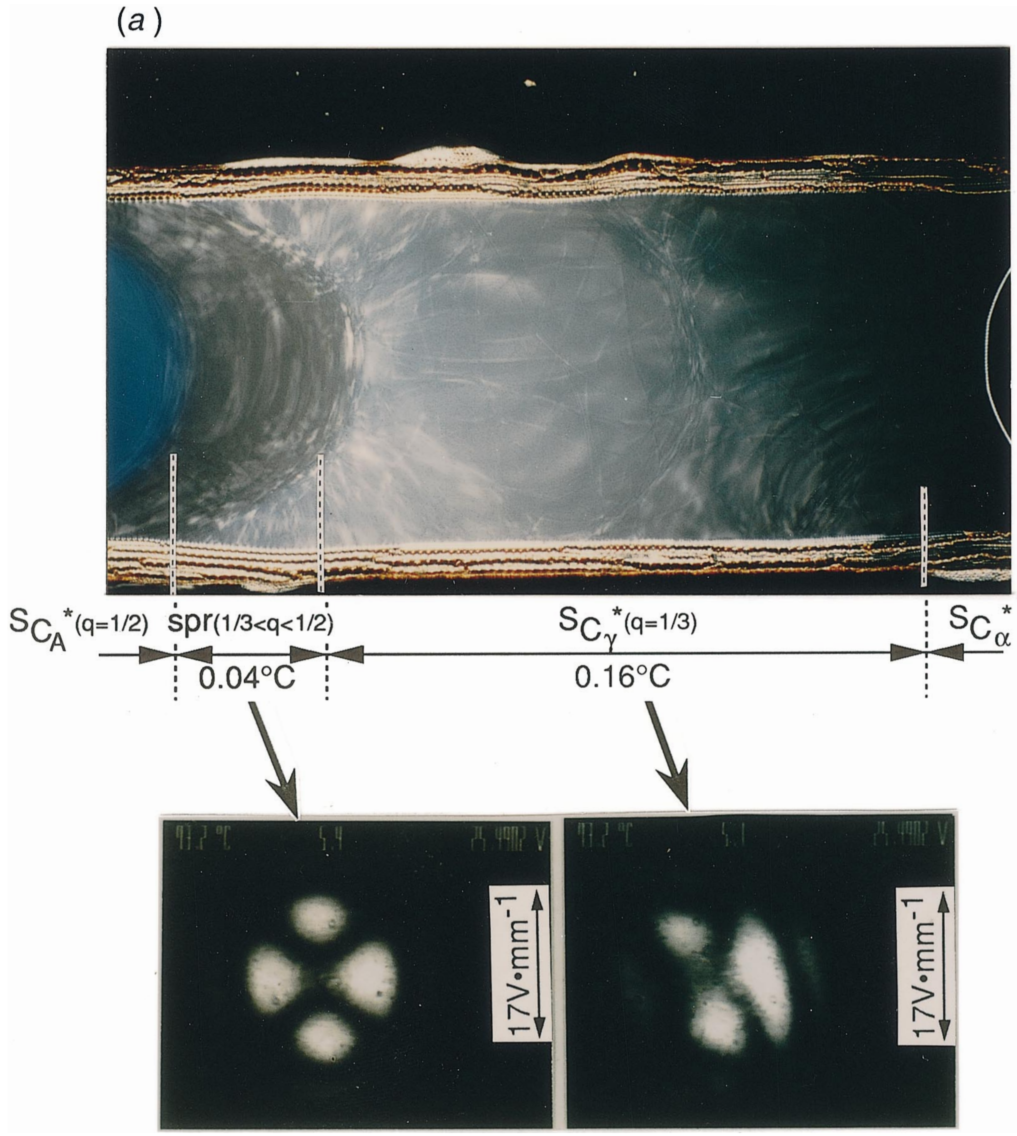

Plate 4 Micrographs of *ca.* 100 μm thick, TFMHPBC free-standing films under temperature gradients, and conoscopic figures of a subphase in spr3 ($1/2>q>1/3$) and SC_γ* ($q=1/3$) under applied electric fields, 17 V mm^{-1}; (*a*) for $R:S=96:4$ and (*b*) for $R:S=92:8$. A subphase in spr2 ($1/3>q>1/4$) is also observed on the right side of (*b*), although no detailed study was performed.

the electric interaction between permanent dipole moments proposed so far for the stabilization of SC_A*, the pairing model by Takanishi *et al.*[22] and the P_x model by Miyachi *et al.*,[66] assure that the molecular tilting occurs in the same direction but in the opposite senses in adjacent layers, although the third model based on the steric interaction in adjacent layers[67] may not be able to do so. In this way, it seems to be well founded to treat the observed sequence of subphases in terms of the frustration between ferroelectricity and antiferroelectricity based on the Ising model. Statistical mechanics models illustrating two different ways of lifting the degeneracy have been developed: the one by weak long-range forces is the one-dimensional Ising model proposed by Bak and Bruinsma[26,27] and the other by thermal effects is the so-called ANNNI (axial next-nearest neighbour Ising) model with competing nearest and next-nearest neighbour coupling proposed by Bak and von Boem.[35]

Trying to simply interpret the observed sequence of the subphases in terms of the Bak–Bruinsma Ising model with the long-range repulsive interactions, we assigned Ising spins to the orderings, ferroelectric (F) and antiferroelectric (A), but not to the tilting senses, right (R) and left (L);[2,9,22] we also considered that, following Bruinsma and Prost,[28] fluctuations of C-directors and hence of spontaneous polarizations cause the long-range repulsive interactions. However, the repulsive interactions between separate F orderings seem to be rather artificial and several difficulties have been noted so far.[2] In fact, Bruinsma and Prost,[28] based on the fluctuation forces, actually showed the emergence of the electric-field-induced Devil's staircase which can be described by the tilting senses,

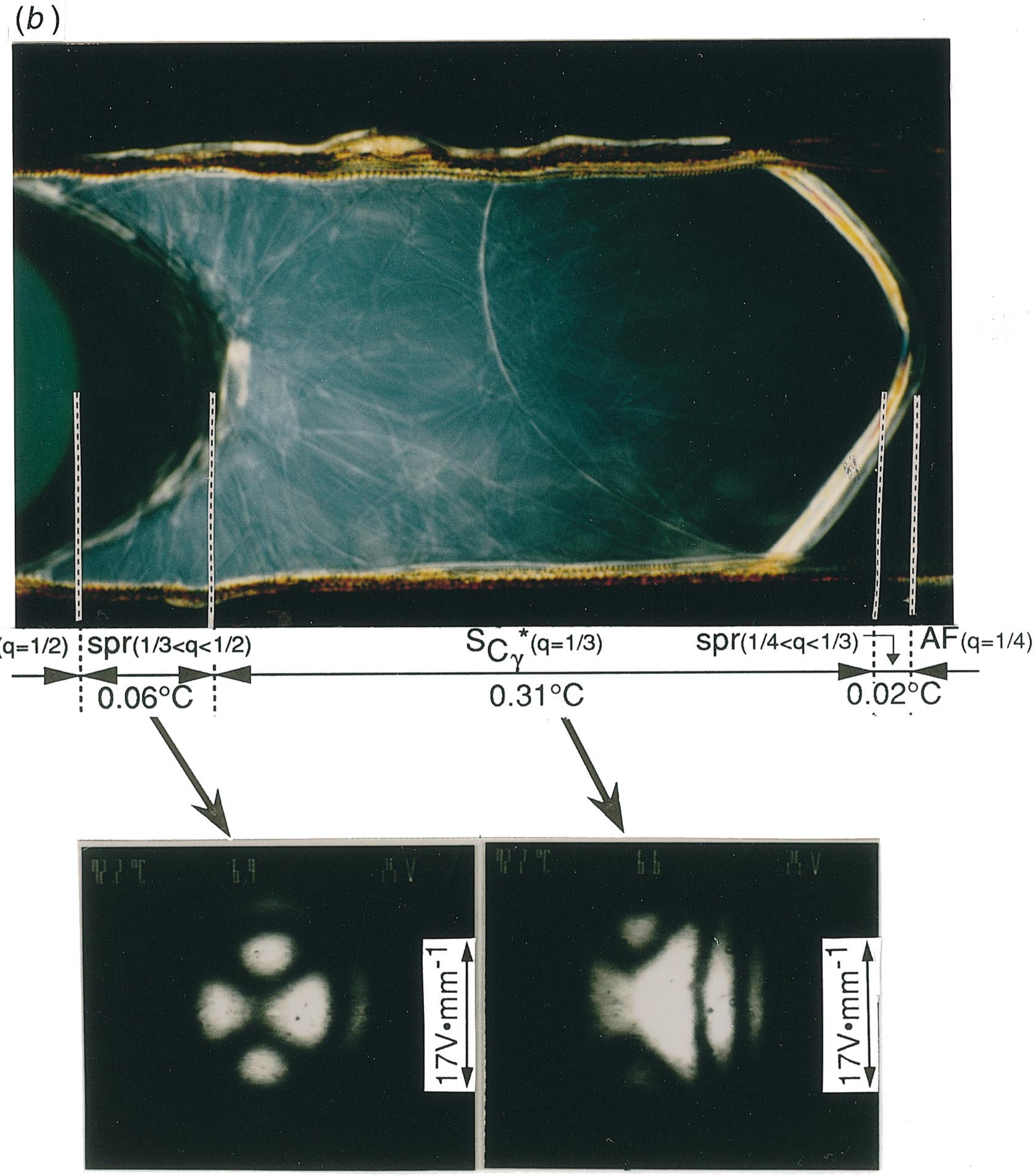

Plate 4 (*continued*)

R and *L*, but not that of the temperature-induced one. Moreover, the stability of subphases changes critically from material to material, although the Bak–Bruinsma Ising model predicts rather universal stability.[26,27] Another issue raised is that no finite temperature effect is taken into account and hence the model can describe only the ground states.[50]

The ANNNI + J_3 model[36] was applied to this problem by Yamashita and Miyazima[29] and by Yamashita.[30,31] The Hamiltonian they assumed is

$$\mathcal{H} = -J \sum_{(i,j)} s_i s_j - J_1 \sum_i^A s_i s_{i+1} - J_2 \sum_i^A s_i s_{i+2} - J_3 \sum_i^A s_i s_{i+3}$$

where the Ising spin s_i takes a value of ± 1 corresponding to the molecular tilting senses of the *i*th smectic layer, the first summation is taken all over nearest-neighbouring pairs (*i*, *j*) in the same smectic layer, and other summations Σ^A are only for the first, second and third neighbouring pairs in the axial direction parallel to the layer normal; the second-nearest neighbour interaction J_2 should be negative to ensure competition, and the third-nearest neighbour interaction J_3 (>0 or <0) is included for the possible wide stability of SC_γ*. Although they did not show any realistic physical grounds for these rather long-range interactions initially, Yamashita[32–34] quite recently claimed an important role played by the sense of the molecular long axis, decimated in the partition function the pseudo-spins describing the senses of molecular long axes, and eventually obtained the effective long-range interactions, J_2, J_3, *etc.*

Such a freedom was already introduced by Koda and Kimura[37,38] to induce negative J_2, who also quite recently extended their theoretical treatment and tried to interpret the observed sequence of subphases and the stability ranges.[39] Their

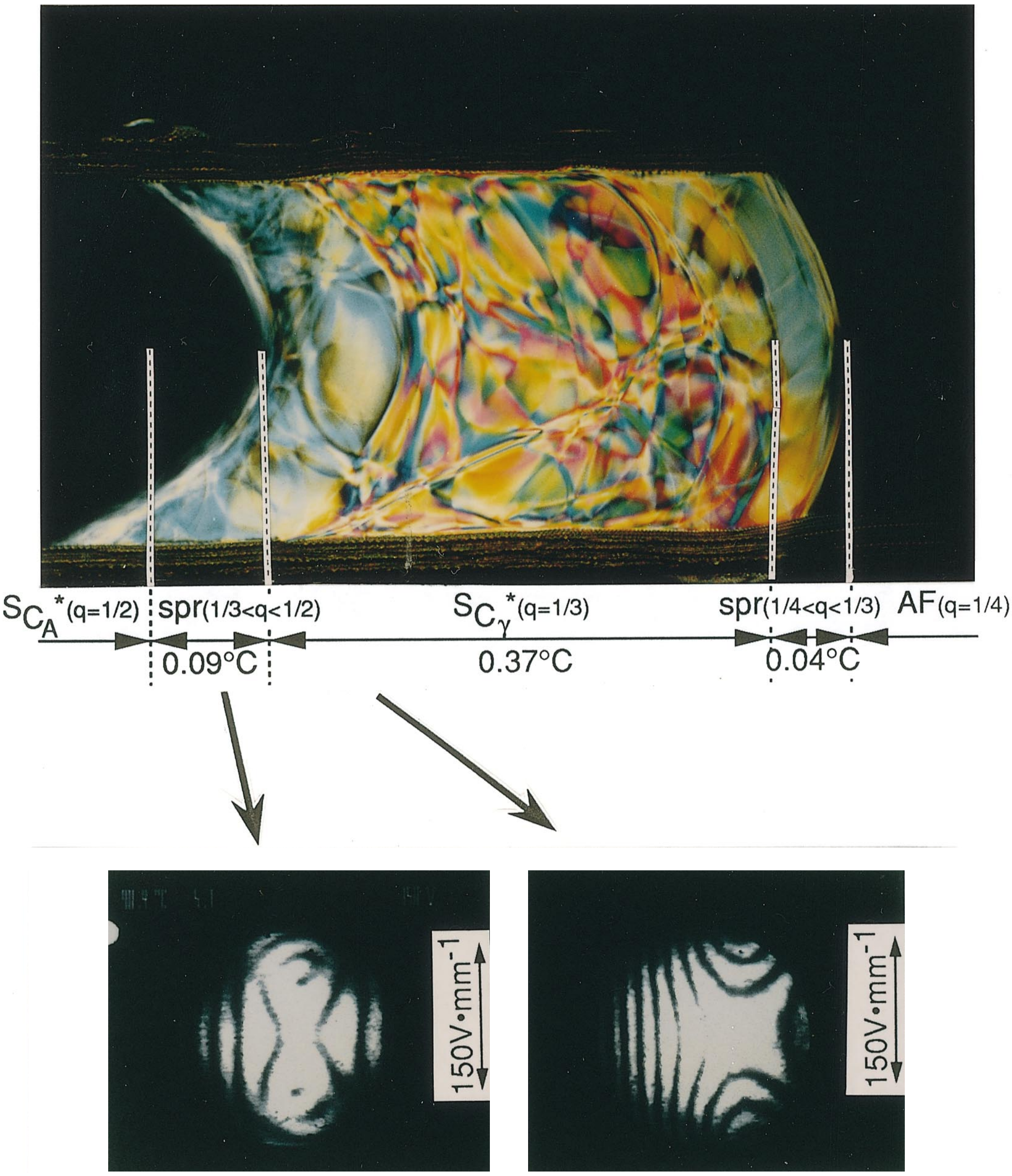

Plate 5 A micrograph of a TFMHPBC ($R:S=88:12$) free-standing film under a temperature gradient, and two conoscopic figures of a subphase in spr3 ($1/2>q>1/3$) and SC_γ* ($q=1/3$), respectively. Some spurious phase boundaries appear; the boundary characterizing a phase in spr2 ($1/3>q>1/4$) on the right side seems to be real, although a conoscopic study was not performed.

method is essentially equivalent to the ANNNI + J_3 model. Yamashita[34] showed that four ground states are SC_A* ($q=1/2$), SC_γ* ($q=1/3$), AF ($q=1/4$) and SC* ($q=0$) as illustrated in Fig. 7. He predicted rather stable ferrielectric phases $q=2/5$ and 4/11 in spr3, $q=4/13$ and 2/7 in spr2, and $q=2/9$ and 1/5 in spr1, estimating the average of the saturated ordering,

$$\sigma=\sum_{i=1}^{p}\frac{\langle s_i\rangle}{p}$$

which is considered to be proportional to the apparent tilt angle, *i.e.* the spontaneous polarization. The estimated ratio of this value to that in SC_γ* ($q=1/3$) is *ca.* 0.6 for $q=2/5$ and *ca.* 0.27 for $q=4/11$. The subphase in spr3 observed in Plate 2 and Fig. 6 is therefore identified as $q=2/5$. The ratio is suggested to be very small for $q=2/9$ and 1/5, and this smallness may explain the characteristic field dependence of the conoscopic figure for the subphase in spr1 observed in Plate 3. It exhibits ferrielectric-like behaviour at low fields, but a secondary interaction through dielectric anisotropy prevails at high fields, resulting in the antiferroelectric conoscopic figure. Yamashita also predicted antiferroelectric phases, $q=3/8$, $q=3/10$ and $q=3/14$, in spr3, spr2 and spr1, respectively.

Conclusions

In this way, the ANNNI + J_3 model,[29–34,36] is flexible enough to explain a variety of observed phase sequences between SC_A* and SC*. For detailed comparison of theory with experiment,

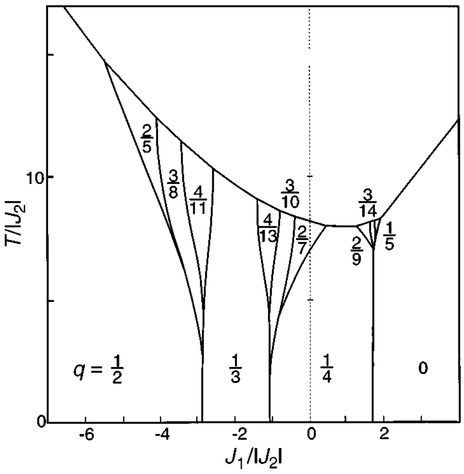

Fig. 7 A phase diagram obtained by the ANNNI+J_3 model for $J_1/|J_2|=1$ and $J_3/|J_2|=0.3$. By courtesy of M. Yamashita.[29–34]

a much more systematic determination of the apparent tilt angle and helicoidal pitch in spr3, spr2, and spr1 needs to be performed with improved accuracy using free-standing films. Some refinement is also necessary in the theoretical treatment. Although Koda and Kimura[39] considered that the polar angle is fluctuating, the azimuthal angle is much more liable to fluctuate and has the first claim to consideration; the tilt angle decrease toward SA should also be taken into account. These refinements may allow us to understand not only the variety of observed phase sequences between SC_A* and SC* but also SC_α*[2,22–24] and the V-shaped switching due to thresholdless antiferroelectricity disclosed recently.[68–71]

We are grateful to Mamoru Yamashita, Kou Tokumaru and Sauseong Seomun for stimulating discussions and for allowing us to use Fig. 7. This work was supported by a Grant-in-Aid for Scientific Research (Specially Promoted Research No. 06102005) from Monbusho in Japan.

References

1 A. D. L. Chandani, E. Gorecka, Y. Ouchi, H. Takezoe and A. Fukuda, *Jpn. J. Appl. Phys.*, 1989, **28**, L1265.
2 A. Fukuda, Y. Takanishi, T. Isozaki, K. Ishikawa and H. Takezoe, *J. Mater. Chem.*, 1994, **4**, 997.
3 M. Fukui, H. Orihara, Y. Yamada, N. Yamamoto and Y. Ishibashi, *Jpn. J. Appl. Phys.*, 1989, **28**, L849.
4 K. Hiraoka, A. D. L. Chandani, E. Gorecka, Y. Ouchi, H. Takezoe and A. Fukuda, *Jpn. J. Appl. Phys.*, 1990, **29**, L1473.
5 J. W. Goodby, J. S. Patel and E. Chin, *J. Mater. Chem.*, 1992, **2**, 197.
6 I. Nishiyama, E. Chin and J. W. Goodby, *J. Mater. Chem.*, 1993, **3**, 161.
7 J. W. Goodby, I. Nishiyama, A. J. Slaney, C. J. Booth and K. J. Toyne, *Liq. Cryst.*, 1993, **14**, 37.
8 T. Isozaki, T. Fujikawa, H. Takezoe, A. Fukuda, T. Hagiwara, Y. Suzuki and I. Kawamura, *Jpn. J. Appl. Phys.*, 1992, **31**, L1435.
9 T. Isozaki, T. Fujikawa, H. Takezoe, A. Fukuda, T. Hagiwara, Y. Suzuki and I. Kawamura, *Phys. Rev. B*, 1993, **48**, 13439.
10 T. Isozaki, H. Takezoe, A. Fukuda, Y. Suzuki and I. Kawamura, *J. Mater. Chem.*, 1994, **4**, 237.
11 T. Isozaki, K. Ishikawa, H. Takezoe and A. Fukuda, *Ferroelectrics*, 1993, **147**, 121.
12 J. Hatano, M. Sato, K. Iwauchi, T. Tsukamoto, S. Saito and K. Murashiro, *Ferroelectrics*, 1993, **147**, 217.
13 H. Hatano, Y. Hanakai, H. Furue, H. Uehara, S. Saito and K. Muraoka, *Jpn. J. Appl. Phys.*, 1994, **33**, 5498.
14 H. Moritake, N. Shigeno, M. Ozaki and K. Yoshino, *Liq. Cryst.*, 1993, **14**, 1283.
15 H. Moritake, M. Ozaki, H. Taniguchi, K. Satoh and K. Yoshino, *Jpn. J. Appl. Phys.*, 1994, **33**, 5503.
16 P. Gisse, J. Pavel, H. T. Nguyen and V. L. Lorman, *Ferroelectrics*, 1993, **147**, 27.
17 P. Cluzeau, H. T. Nguyen, Ch. Destrade, N. Isaert, P. Barois and A. Babeau, *Mol. Cryst. Liq. Cryst.*, 1995, **260**, 69.
18 M. Glogarova, H. Svorenyak, H. T. Nguen and Ch. Destrade, *Ferroelectrics*, 1993, **147**, 37.
19 T. Sako, Y. Kimura, R. Hayakawa, N. Okabe and Y. Suzuki, *Jpn. J. Appl. Phys.*, 1996, **35**, L114.
20 Yu. P. Panarin, H. Xu, S. T. MacLughadha, J. K. Vij, A. J. Seed, M. Hird and J. W. Goodby, *J. Phys.: Condens. Matter*, 1995, **7**, L351.
21 J. W. O'Sullivan, Yu. P. Panarin and J. K. Vij, *Poster Presentation at 16th Int. Liq. Cryst. Conf.* (*Kent*, *1996*), C1P.15 (P-125).
22 Y. Takanishi, K. Hiraoka, V. K. Agrawal, H. Takezoe, A. Fukuda and M. Matsushita, *Jpn. J. Appl. Phys.*, 1991, **30**, 2023.
23 K. Hiraoka, Y. Takanishi, K. Skarp, H. Takezoe and A. Fukuda, *Jpn. J. Appl. Phys.*, 1991, **30**, L1819.
24 T. Isozaki, K. Hiraoka, Y. Takanishi, H. Takezoe, A. Fukuda, Y. Suzuki and I. Kawamura, *Liq. Cryst.*, 1992, **12**, 59.
25 M. Neundorf, Y. Takanishi, A. Fukuda, S. Saito, K. Murashiro, T. Inukai and D. Demus, *J. Mater. Chem.*, 1995, **5**, 2221.
26 P. Bak and R. Bruinsma, *Phys. Rev. Lett.*, 1982, **49**, 249.
27 R. Bruinsma and P. Bak, *Phys. Rev. B.*, 1983, **27**, 5824.
28 R. Bruinsma and J. Prost, *J. Phys. II* (*France*), 1994, **4**, 1209.
29 M. Yamashita and S. Miyazima, *Ferroelectrics*, 1993, **148**, 1.
30 M. Yamashita, *Mol. Cryst. Liq. Cryst.*, 1995, **263**, 93.
31 M. Yamashita, *Ferroelectrics*, 1996, **181**, 201.
32 M. Yamashita, *J. Phys. Soc. Jpn.*, 1996, **65**, 2122.
33 M. Yamashita, *J. Phys. Soc. Jpn.*, 1996, **65**, 2904.
34 M. Yamashita, *Poster Presentation at 16th Int. Liq. Cryst. Conf. (Kent, 1996)*, C1P.12 (P-124), *Mol. Cryst. Liq. Cryst.*, to be published.
35 P. Bak and J. von Boem, *Phys. Rev. B*, 1980, **21**, 5297.
36 Y. Yamada and N. Hayama, *J. Phys. Soc. Jpn.*, 1983, **52**, 3466.
37 T. Koda and H. Kimura, *Ferroelectrics*, 1993, **148**, 31.
38 T. Koda and H. Kimura, *J. Phys. Soc. Jpn.*, 1995, **64**, 3787.
39 T. Koda and H. Kimura, *J. Phys. Soc. Jpn.*, 1996, **65**, in press.
40 M. Nakagawa, *J. Phys. Soc. Jpn.*, 1993, **62**, 2260.
41 H. Orihara and Y. Ishibashi, *Jpn. J. Appl. Phys.*, 1990, **29**, L115.
42 H. Orihara and Y. Ishibashi, *Jpn. J. Appl. Phys.*, 1990, **30**, L1819.
43 H. Sun, H. Orihara and Y. Ishibashi, *J. Phys. Soc. Jpn.*, 1991, **60**, 4175.
44 H. Sun, H. Orihara and Y. Ishibashi, *J. Phys. Soc. Jpn.*, 1993, **62**, 2706.
45 B. Zeks, R. Blinc and M. Cepic, *Ferroelectrics*, 1991, **122**, 221.
46 B. Zeks and M. Cepic, *Liq. Cryst.*, 1993, **14**, 445.
47 M. Cepic, G. Heppke, J-M. Hollidt, D. Lotzsch and B. Zeks, *Ferroelectrics*, 1993, **147**, 159.
48 M. Cepic, G. Heppke, J-M. Hollidt, D. Lotzsch, D. Moro and B. Zeks, *Mol. Cryst. Liq. Cryst.*, 1995, **263**, 207.
49 M. Cepic and B. Zeks, *Mol. Cryst. Liq. Cryst.*, 1995, **263**, 61.
50 S. A. Pikin, S. Hiller and W. Haase, *Mol. Cryst. Liq. Cryst.*, 1995, **262**, 425.
51 V. L. Lorman, A. A. Bulbitch and P. Toledano, *Phys. Rev. E*, 1994, **49**, 1367.
52 V. L. Lorman, *Mol. Cryst. Liq. Cryst.*, 1995, **262**, 437.
53 X. Y. Wang and P. L. Taylor, *Phys. Rev. Lett.*, 1996, **76**, 640.
54 C. Y. Young, R. Pindak, N. A. Clark and R. B. Meyer, *Phys. Rev. Lett.*, 1978, **40**, 773.
55 Ch. Bahr and D. Fliegner, *Phys. Rev. Lett.*, 1993, **70**, 1842.
56 Ch. Bahr and D. Fliegner, *Ferroelectrics*, 1993, **147**, 1.
57 Y. Saito, C-C. Chou, K. Morita, H. Takezoe, A. Fukuda, H. Mori and M. Gokudan, *Proc. SID*, 1991, **32**, 213.
58 T. Fujikawa, K. Hiraoka, T. Isozaki, K. Kajikawa, H. Takezoe and A. Fukuda, *Jpn. J. Appl. Phys.*, 1993, **32**, 985.
59 S. Garoff and R. B. Meyer, *Phys. Rev. A*, 1979, **19**, 338.

60 K. Yamada, K. Miyachi, Y. Takanishi, K. Ishikawa, H. Takezoe and A. Fukuda, *Extended Abstracts of 43th Spring Meeting of Jpn. Soc. Appl. Phys. and Related Societies*, Toyo University, Saitama, 1996, 28 aZP/III-2.
61 E. Gorecka, A. D. L. Chandani, Y. Ouchi, H. Takezoe and A. Fukuda, *Jpn. J. Appl. Phys.*, 1990, **29**, 131.
62 Y. Takanishi, M. Kabe, H. Takezoe and A. Fukuda, *Phys. Rev.*, submitted.
63 K. Miyachi, M. Kabe, K. Ishikawa, H. Takezoe and A. Fukuda, *Ferroelectrics*, 1993, **147**, 147.
64 J. Li, H. Takezoe and A. Fukuda, *Jpn. J. Appl. Phys.*, 1991, **30**, 532.
65 H. Takezoe, J. Lee, Y. Ouchi and A. Fukuda, *Mol. Cryst. Liq. Cryst.*, 1991, **202**, 85.
66 K. Miyachi, J. Matsushima, Y. Takanishi, K. Ishikawa, H. Takezoe and A. Fukuda, *Phys. Rev. E*, 1995, **52**, R2153.
67 I. Nishiyama and J. W. Goodby, *J. Mater. Chem.*, 1992, **2**, 1015.
68 S. Inui, N. Iimura, T. Suzuki, H. Iwane, K. Miyachi, Y. Takanishi and A. Fukuda, *J. Mater. Chem.*, 1996, **6**, 671.
69 A. Fukuda, *Proc. 15th Int. Display Research Conf.* Hamamatsu, 1995, S6-1, p. 61.
70 A. Fukuda, S. S. Seomon, T. Takahashi, Y. Takanishi and K. Ishikawa, *Invited Lecture at 16th Int. Liq. Cryst. Conf.* (*Kent, 1996*), E2.I01 (155), *Mol. Cryst. Liq. Cryst.*, to be published.
71 T. Saishu, K. Takatoh, R. Iida, H. Nagata and Y. Mori, *SID '96 Digest* [Ext. Abstr. Int. Symposium, Seminar, & Exhibition (San Diego, 1996)], 28.4.

Paper 6/05942B; *Received* 28*th August*, 1996